J. Chem. Sci. (2020) 132:150
https://doi.org/10.1007/s12039-020-01851-9

REGULAR ARTICLE

Opto-electrochemistry of pyridopyrazino[2,3-*b*]indole Derivatives

POOJA S SINGH, AKSHATA J SHIRGAONKAR, BHARGAVI K CHAWATHE and RAJESH M KAMBLE*

Department of Chemistry, University of Mumbai, Santacruz (E), Mumbai 400 098, India
E-mail: kamblerm@chem.mu.ac.in

MS received 25 June 2020; revised 22 August 2020; accepted 4 September 2020

Abstract. Here, pyridopyrazino[2,3-*b*]indole based D–A assembly was designed and synthesized with modulation of various electron-donating/withdrawing substituent and characterized by various spectroscopic methods. Pyridopyrazino[2,3-*b*]indole derivatives show inbuilt intramolecular charge transfer (ICT) transition which established D–A building in molecules and induces blue-green emission in the solution state. However, solid-state emission characteristics explore the emission property of some molecules towards aggregation-induced emission (AIE) effect which leads to the formation of emissive nano aggregates in THF/H_2O mixture. Alteration of substituent on pyridopyrazino[2,3-*b*]indole segment effectively tune electrochemical property and resulting LUMO energy level was found to be comparable with reported electron transporting/n-type materials. These properties and good thermal stability indicate that molecules have the potential to be used as solid-state emitter and n-type materials in optoelectronic devices.

Keywords. Pyridopyrazino[2,3-*b*]indole; intramolecular charge transfer; donor–acceptor; HOMO–LUMO energy level; aggregation-induced emission; n-type materials.

1. Introduction

In recent years, smaller heterocyclic compounds having donor–acceptor (D–A) interaction set up one of the largest areas of research in organic electronics[1–3] due to their tuneable optoelectronic property, well–defined structures, ease of purification, solubility in a wide range of organic solvents, thermal stability and low-cost solution processing techniques.[4] In addition, intramolecular charge transfer (ICT) feature of these systems is advantageous to tune the required luminescence in a molecule. However, a major drawback of D–A molecules having disc-like shape/planar geometry is quenched emission in concentrate/aggregate/solid-state which leads to aggregation-caused quenching (ACQ) phenomenon.[5,6] Planar geometry of such system increases intermolecular π–π stacking interactions which arouse the non-radiative relaxation process. Hence, this debases the solid-state emission of the molecule which is generally required for the construction of highly efficient non-doped organic light-emitting diodes (OLED's) or bio-imaging application.[1,7] Hence Tang and his co-worker proposed a novel idea of "aggregation-induced emission" (AIE)[8] which can tackle the problem associated with an ACQ effect by a strategy of restricted intramolecular rotation (RIR) and conformational changes of molecules in its aggregate state. Tang suggests, AIE, usually observed in non-planar, propeller-shaped luminogens that were almost non-fluorescent in solution, became highly fluorescent on aggregation or in solid-state.[9,10] Thus, AIE broadens the applicative area of D–A molecules in organic electronic devices, mainly in OLED's as solid-state emissive materials.

Furthermore, being an indispensable component of the integrated circuit, n-type/electron-transporting materials (ETM) can improve the stability and power efficiency of organic semiconducting devices and hence there is an urgent demand of ETM over p-type/hole-transporting materials (HTM). On the other hand, difficult synthetic approach and poor stability of ETM under ambient conditions delimits their availability in these fields. However, past report suggests, ETM can be simply designed from HTM

*For correspondence

Electronic supplementary material: The online version of this article (https://doi.org/10.1007/s12039-020-01851-9) contains supplementary material, which is available to authorized users.

Published online: 07 November 2020

material by the insertion of smaller groups like –F, –CN, –Cl, $–NO_2$, –COOH, etc., or N-atom in the structural core of a molecule.[11,12] According to the previous report, numerous small D–A architecture based carbazole,[13,14] quinoxaline,[15–22] indolo-quinoxaline,[23–27] pyrido-pyrazine,[28,29] phenazine[30–32] derivatives were studied and utilized for application in organic electronics due to its excellent semiconducting, emissive property in solution or solid-state and also known for its outstanding AIE characteristics.

Besides these, pyridopyrazino[2,3-*b*]indole derivatives are one of the important class of nitrogen-containing heterocyclic compounds. However, a major shortcoming in the synthesis of these compounds is the formation of regioisomers as suggested by Buu-Hoi and Saint-Ruf in 1960 for the first time.[33] They obtained two regioisomeric compounds of pyridopyrazino[2,3-*b*]indole i.e., **a** and **b** by heating reaction mixture of non-symmetric pyridine-2,3-diamines reactant and isatin in ethanol, but preference to the formation of the major product was given to the former one without any spectroscopic evidence (Chart 1).[33]

Later on Bergman *et al.,* obtained this two regioisomers (**a** and **b**) in the ratio of 2:1 by simply heating the reaction mixture containing isatin and pyridine-2,3-diamine for 3 h in acetic acid and for the first time provided valid spectroscopic data for characterization of these two regioisomers (Chart 1).[34] Instead, the same reaction carried out in ethanol solvent gave several by-products along with these two regioiosmers which delimits the use of it in the synthesis of pyridopyrazino[2,3-*b*]indole.[34] With the continuity of Bergman's work, Andrieu *et. al.,* came up with two different tedious methods for the production of N-alkylated (NH group of indole segment) derivative of pyridopyrazino[2,3-*b*]indole regioisomers and successfully characterised both the product through spectroscopic technique.[35]

Further, some more reports on the synthesis of pyridopyrazino[2,3-*b*]indole derivatives are found in literature[36–38] and its biological activity as an anti-amoebic agent was studied in 1976 by Seth *et. al.*[39] However, to the best of our knowledge, optoelectronic and thermal properties of pyridopyrazino[2,3-*b*]indole and their derivatives have not been studied till date. As pyridopyrazino[2,3-*b*]indole having additional pyridine N-atoms in the fused ring of the molecular framework than that of indolo-quinoxaline and hence may exhibit higher electron-accepting ability than indolo-quinoxaline. In addition, the presence of strong electron-donating (indole analog) and accepting (pyrido-pyrazine analog) property within a molecule may exhibit unique charge transfer characteristics and hence could be advantageous for their application in optoelectronics.

Thus, herein we decided to synthesize a series of pyridopyrazino[2,3-*b*]indole derivatives **1–10** containing –Br, –Cl, $–CH_3$ and $–NO_2$ substituents and studied their detail photophysical, electrochemical and thermal properties. The synthetic route adopted for target compounds **1–10** is shown in Scheme 1 and molecular structure of **1–10** presented in Chart 2. The identity and purity of desired molecules were confirmed by FT-IR, ^1H, ^{13}C NMR spectroscopy, MALDI-Tof spectrometry and elemental analysis.

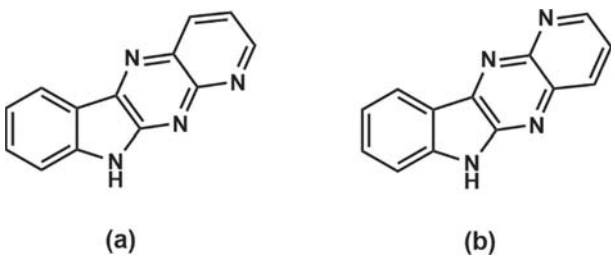

Chart 1. Plausible pyridopyrazino[2,3-*b*]indole regioisomers formed by the reaction of isatin with pyridine-2,3-diamine in acetic acid/ethanol.

2. Experimental

2.1 *Materials and methods*

All materials were purchased from commercial sources as Sigma Aldrich and Alfa Aesar, used without any further purification. The organic solvents (HPLC and spectroscopic grade) were dried using standard procedures and handled in a moisture-free atmosphere. SD Fine silica gel (60–120 mesh) was used for column chromatography with n-hexane and chloroform as eluent. Thin-layer chromatography (TLC) was used to monitor the progress of reactions and purity of the compounds were visualized with UV light (365 nm) and in an iodine chamber. The melting point was measured by an open capillary method. ^1H and ^{13}C NMR spectra were recorded on a Bruker 300 Ultrashield spectrometer (300 and 75 MHz, respectively) in $CDCl_3$ with TMS as an internal standard. Fourier transforms infrared (FT–IR) spectra were recorded using a solid powder sample on a Perkin Elmer Frontier 91579. Mass spectrometric measurements were recorded using MALDI–TOF (Bruker) and elemental analysis was performed on an EA Euro–elemental analysis instrument. UV–Visible spectra recorded in 10^{-5} mole L^{-1} solutions and solid film on a SHIMADZU UV–2401PC at room temperature. Solid films (6 mg mL^{-1} sample in chloroform) prepared on a quartz glass plate using spin coater (Holmarc HO–TH–05) at 1000

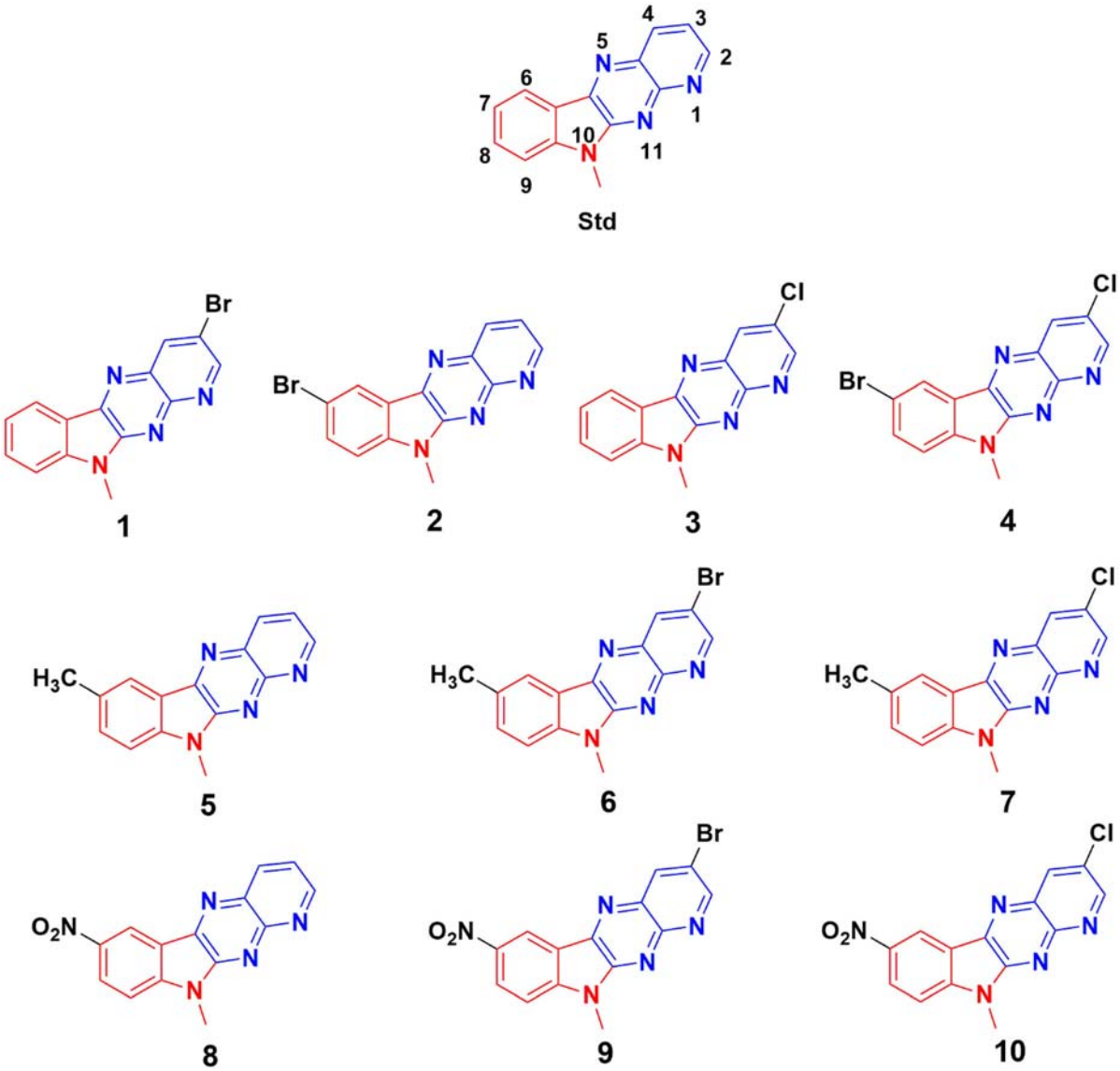

Chart 2. Molecular structures of **Std** and **1**–**10**.

rpm for 2 min. The emission spectra were measured on SHIMADZU RF–5301PC fluorescence spectrophotometer. Hydrodynamic particle sizes were obtained by DLS analysis using Zetasizer(7.12)–MAL1180779. TGA was performed on a Metler–Toledo instrument under nitrogen atmosphere. Cyclic voltammetry studies were carried out on a computer-controlled PalmSens3 potentiostat or galvanostat instrument. Typically, a three-electrode cell equipped with a glassy carbon working electrode, Ag/AgCl (non-aqueous) reference electrode and platinum (Pt) wire counter electrode was employed. The measurements were carried out with a scan rate of 100 mVs^{-1} at room temperature in anhydrous DCM with Tetrabutylammonium hexafluorophosphate (TBHP) solution (0.1 M) as supporting electrolyte. The potential of the Ag/AgCl reference electrode was calibrated using the ferrocene/ferrocenium redox couple with the known oxidation potential of +5.1 eV.

2.2 *Synthetic procedure*

2.2a *Alkylation of Isatin derivatives*: Methylation at indole nitrogen of isatin (indoline-2,3-dione) and its derivatives having substituted –Br, $–CH_3$ and $–NO_2$ groups were done according to a procedure described by Beauchard et al. (2006) to increase the solubility of the final product in common organic solvents.[40]

2.2b *Synthesis of 10-methyl-10H-pyrido[3′,2′:5,6] pyrazino[2,3-b]indole (**Std**)′*: Synthesis of **Std** molecule was previously reported by Andrieu and Mdrour in 1998 which is quite tedious method and give two regioisomers.[35] However preparative method adopted for the synthesis of non-alkylated **Std** molecule i.e., 10*H*-pyrido[3′,2′:5,6]pyrazino[2,3-*b*]indole (molecule **a** given in Chart 1) by Bergman is relatively easier using glacial

acetic acid as a solvent and can give desired molecule (**Std**) as a predominate product from the two regioisomers formed.[34] So, **Std** molecule was prepared by simply condensing or refluxing a mixture of 1-methylindoline-2,3-dione (200 mg, 1 mmol) and pyridine-2,3-diamine (140 mg, 1 mmol) in glacial acetic acid (20 mL) for 3 h. Afterwards, the reaction mixture was allowed to cool and then poured onto crushed ice to obtain the crude solid which was purified using column chromatography (eluent n-hexane:chloroform). Like previous reports on pyridopyrazino[2,3-*b*]indole,[33,34] after purification, we also got the desired product as a major compound and another one as a minor product. The formation of desired product (**Std**) was confirmed by its melting point (Lit. M.p.: 222–224 °C),[35] ^{1}H, ^{13}C NMR, IR, mass spectrum and elemental analysis. Red solid. Yield: 0.235 g (81.46%); M.p.: 221 °C (Lit. M.p.: 222–224 °C);[35] FT-IR (solid, ν_{max}/cm^{-1}): 3054 (Ar. =C–H str.), 2971; 2920; 2840 (Aliph. –C–H str.), 1673 (Ar. –C=N str.), 1596; 1451(Ar. –C=C str.), 1326 (C–N str.), 1069; 746 (Ar. –C–H bend); ^{1}H NMR (300 MHz, $CDCl_3$, 25 °C) δ, ppm: 8.93 (dd, 1H, H-2, *J* = 2.4 Hz, 2.7 Hz), 8.56 (dd, 1H, H-4, *J* = 2.4 Hz, 2.4 Hz), 8.32 (d, 1H, ArH, *J* = 7.5 Hz), 7.73–7.67 (m, 2H, ArH), 7.58 (d, 1H, ArH, *J* = 7.5 Hz), 7.40 (t, 1H, H-3, *J* = 7.5 Hz), 3.93 (s, 3H, N($C\underline{H}_3$)); ^{13}C NMR (75 MHz, $CDCl_3$, 25 °C) δ, ppm: 152.68, 149.82, 148.87, 146.68, 138.76, 135.26, 134.33, 132.11, 123.28, 122.28, 121.65, 119.15, 109.66, 28.28 (N($\underline{C}H_3$)); MALDI-TOF: mass calcd. for $C_{14}H_{10}N_4$ $[M]^+$: 234.26; found $[M]^+$: 234.65; Elemental anal. calcd. for $C_{14}H_{10}N_4$: C, 71.78; H, 4.30; N, 23.92% Found: C, 71.74; H, 4.34; N, 23.90%.

2.2c *Preparation of pyridopyrazino[2,3-b]indole derivatives (**1–10**)*

*2.2.2a. b 3-bromo-10-methyl-10H-pyrido[3′,2′:5,6]pyrazino[2,3-b]indole (**1**)* Similar condensation procedure as for **Std** starting from 1-methylindoline-2,3-dione (200 mg, 1 mmol) and 5-bromopyridine-2,3-diamine (233 mg, 1 mmol). Green solid. Yield: 0.253 g (65.24%); M.p.: 282 °C; FT-IR (solid, ν_{max}/cm^{-1}): 3055 (Ar. =C–H str.), 2966; 2852 (Aliph. –C–H str.), 1673 (Ar. –C=N str.), 1598; 1476 (Ar. –C=C str.), 1397 (C–N str.), 1254; 1115; 1083; 743 (Ar. –C–H bend), 884 (C–Br); ^{1}H NMR (300 MHz, $CDCl_3$, 25 °C) δ, ppm: 9.03 (d, 1H, H-2, *J* = 2.4 Hz), 8.32 (d, 1H, H-4, *J* = 7.5 Hz), 7.73–7.67 (m, 2H, ArH), 7.42–7.35 (m, 2H, ArH), 3.94 (s, 3H, N($C\underline{H}_3$)); ^{13}C NMR (75 MHz, $CDCl_3$, 25 °C) δ, ppm: 152.98, 150.32, 145.84, 141.76, 139.40, 137.75, 133.93, 132.21, 123.87, 122.92; 122.01, 116.49, 109.83, 28.57 (N($\underline{C}H_3$)); MALDI-TOF: mass calcd for $C_{14}H_9BrN_4$ $[M]^+$: 313.15; found $[M]^+$: 313.12, [M+2]: 315.48; Elemental anal. calcd. for $C_{14}H_9BrN_4$: C, 53.70; H, 2.90; Br, 25.52; N, 17.89% Found: C, 53.68; H, 2.94; Br, 25.48; N, 17.92%.

*2.2.2b. b 7-bromo-10-methyl-10H-pyrido[3′,2′:5,6]pyrazino[2,3-b]indole (**2**)* Similar condensation procedure as for **Std** starting from 5-bromo-1-methylindoline-2,3-dione (200 mg, 1 mmol) and pyridine-2,3-diamine (120 mg, 1 mmol). Red solid. Yield: 0.206 g (79.28%); M.p.: 198 °C; FT-IR (solid, ν_{max}/cm^{-1}): 3057 (Ar. =C–H str.), 2929; 2852 (Aliph. –C–H str.), 1678 (Ar. –C=N str.), 1586; 1445 (Ar. –C=C str.), 1307 (C–N str.), 1098; 713 (Ar. –C–H bend), 825 (C–Br); ^{1}H NMR (300 MHz, $CDCl_3$, 25 °C) δ, ppm: 8.68 (dd, 1H, H-2, *J* = 1.2 Hz, 1.2 Hz), 8.00 (dd, 1H, H-4, *J* = 1.5 Hz, 1.5 Hz), 7.72 (d, 1H, H-6, *J* = 1.5 Hz), 7.46–7.40 (m, 2H, ArH), 7.37–7.20 (m, 1H, ArH), 3.92 (s, 3H, N($C\underline{H}_3$)); ^{13}C NMR (75 MHz, $CDCl_3$, 25 °C) δ, ppm: 153.24, 152.36, 151.33, 145.65, 145.09, 145.03, 138.41, 134.11, 127.90, 124.25, 120.56, 117.70, 110.03, 29.66 (N($\underline{C}H_3$)); MALDI-TOF: mass calcd for $C_{14}H_9BrN_4$ $[M]^+$: 313.15; found $[M]^+$: 313.17, [M+2]: 315.32; Elemental anal. calcd. for $C_{14}H_9BrN_4$: C, 53.70; H, 2.90; Br, 25.52; N, 17.89% Found: C 53,.73; H, 2.87; Br, 25.54; N, 17.86%.

*2.2.2c. b 3-chloro-10-methyl-10H-pyrido[3′,2′:5,6]pyrazino[2,3-b]indole (**3**)* Similar condensation procedure as for **Std** starting from 1-methylindoline-2,3-dione (200 mg, 1 mmol) and 5-chloropyridine-2,3-diamine (177 mg, 1 mmol). Red solid. Yield: 0.266 g (80.16%); M.p.: 193 °C; FT-IR (solid, ν_{max}/cm^{-1}): 3030 (Ar. =C–H str.), 2925; 2843 (Aliph. –C–H str.), 1674 (Ar. –C=N str.), 1596; 1471 (Ar. –C=C str.), 1333 (C–N str.), 1083; 749 (Ar. –C–H bend), 931 (C–Cl); ^{1}H NMR (300 MHz, $CDCl_3$, 25 °C) δ, ppm: 8.79 (d, 1H, H-2, *J* = 1.2 Hz), 8.24 (d, 1H, H-4, *J* = 1.5 Hz), 7.73–7.67 (m, 2H, ArH), 6.83 (d, 2H, ArH, *J* = 8.4 Hz), 3.95 (s, 3H, N($C\underline{H}_3$)); ^{13}C NMR (75 MHz, $CDCl_3$, 25 °C) δ, ppm: 157.35, 150.03, 148.14, 147.89, 140.62, 138.36, 128.15, 125.15, 123.82, 118.62, 116.50, 111.70, 109.71, 28.65 (N($\underline{C}H_3$)); MALDI-TOF: mass calcd for $C_{14}H_9ClN_4$ $[M]^+$: 268.70; found $[M]^+$: 268.42, [M+2]: 270.57; Elemental anal. calcd. for $C_{14}H_9ClN_4$: C, 62.58; H, 3.38; Cl, 13.19; N, 20.85% Found: C, 62.56; H, 3.40; Cl, 13.23; N, 20.82%.

*2.2.2d. b 7-bromo-3-chloro-10-methyl-10H-pyrido[3′,2′:5,6]pyrazino[2,3-b]indole (**4**)* Similar condensation procedure as for **Std** starting from 5-bromo-1-methylindoline-2,3-dione (200 mg, 1 mmol) and 5-chloropyridine-2,3-diamine (119 mg, 1 mmol). Yellow solid. Yield: 0.174 g (60.58%); M.p.: 241 °C; FT-IR (solid, ν_{max}/cm^{-1}): 3054 (Ar. =C–H str.), 2937; 2885 (Aliph. –C–H str.), 1675 (Ar. –C=N str.), 1601; 1452 (Ar. –C=C str.), 1389 (C–N str.), 1276; 1126; 727 (Ar. –C–H bend), 826 (C–Br), 905 (C–Cl); ^{1}H NMR (300 MHz, $CDCl_3$, 25 °C) δ, ppm: 8.79 (d, 1H, H-2, *J* = 1.2 Hz), 8.24 (d, 1H, H-4, *J* = 1.5 Hz), 7.72 (d, 1H, H-6, *J* = 1.5 Hz), 7.44 (dd, 1H, H-8, *J* = 1.5 Hz, 1.5 Hz), 7.21 (d, 1H, H-9, *J* = 7.5 Hz), 3.91 (s, 3H, N($C\underline{H}_3$)); ^{13}C NMR (75 MHz, $CDCl_3$, 25 °C) δ, ppm: 151.01, 147.35, 147.24, 145.65, 144.12, 141.64, 138.41,

130.70, 130.09, 127.90, 120.56, 117.70, 110.04, 29.66 (N($\underline{C}H_3$)). MALDI-TOF: mass calcd for $C_{14}H_8BrClN_4$ $[M]^+$: 347.60; found $[M]^+$: 347.65, [M+2]: 349.70, [M+4]: 351.75; Elemental anal. calcd. for $C_{14}H_8BrClN_4$: C, 48.37; H, 2.32; Br, 22.99; Cl, 10.20; N, 16.12% Found: C, 48.35; H, 2.36; Br, 22.96; Cl, 10.23; N, 16.09%.

*2.2.2e. b 7,10-dimethyl-10H-pyrido[3′,2′:5,6]pyrazino[2,3-b]indole (**5**)* Similar condensation procedure as for **Std** starting from 1,5-dimethylindoline-2,3-dione (200 mg, 1 mmol) and pyridine-2,3-diamine (100 mg, 1 mmol). Red solid, Yield: 0.283 g (86.35%); M.p.: 172 °C; FT-IR (solid, ν_{max}/cm^{-1}): 3030 (Ar. =C–H str.), 2925; 2843 (Aliph. –C–H str.), 1682 (Ar. –C=N str.), 1611; 1485 (Ar. –C=C str.), 1333 (C–N str.), 1105; 825 (Ar. –C–H bend); ^{1}H NMR (300 MHz, $CDCl_3$, 25 °C) δ, ppm: 8.93 (dd, 1H, H-2, *J* = 2.4 Hz, 2.7 Hz), 8.00 (dd, 1H, H-4, *J* = 1.5 Hz, 1.5 Hz), 7.21–7.05 (m, 2H, Ar-H), 6.87 (d, 1H, H-8, *J* = 7.8 Hz), 6.76 (d, 1H, H-9, *J* = 7.8 Hz), 3.98 (s, 3H, N($\underline{C}H_3$)), 2.31 (s, 3H, –$\underline{C}H_3$); ^{13}C NMR (75 MHz, $CDCl_3$, 25 °C) δ, ppm: 153.04, 151.11, 145.78, 138.78, 136.24, 132.13, 125.16, 124.21, 121.64, 118.52, 117.88, 115.01, 109.95, 28.26 (N($\underline{C}H_3$)), 21.34 (–$\underline{C}H_3$); MALDI-TOF: mass calcd for $C_{15}H_{12}N_4$ $[M]^+$: 248.28; found $[M]^+$: 248.09; Elemental anal. calcd. for $C_{15}H_{12}N_4$: C, 72.56; H, 4.87; N, 22.57% Found: C, 72.54; H, 4.90; N, 22.58%.

*2.2.2f. b 3-bromo-7,10-dimethyl-10H-pyrido[3′,2′:5,6]pyrazino[2,3-b]indole (**6**)* Similar condensation procedure as for **Std** starting from 1,5-dimethylindoline-2,3-dione (200 mg, 1 mmol) and 5-bromopyridine-2,3-diamine (128 mg, 1 mmol). Green solid. Yield: 0.268 g (72.14%); M.p.: >250 °C; FT-IR (solid, ν_{max}/cm^{-1}): 3040 (Ar. =C–H str.), 2926; 2852 (Aliph. –C–H str.), 1683 (Ar. –C=N str.), 1590; 1491 (Ar. –C=C str.), 1385 (C–N str.), 1126; 824 (Ar. –C–H bend), 885 (C–Br); ^{1}H NMR (300 MHz, $CDCl_3$, 25 °C) δ, ppm: 8.96 (d, 1H, H-2, *J* = 1.8 Hz), 8.14 (s, 1H, H-4), 7.53–7.13 (m, 3H, ArH), 3.94 (s, 3H, N($\underline{C}H_3$)), 2.54 (s, 3H, –$\underline{C}H_3$); ^{13}C NMR (75 MHz, $CDCl_3$, 25 °C) δ, ppm: 151.28, 148.77, 144.11, 141.86, 136.37, 134.69, 133.01, 131.42, 128.02, 123.36, 118.59, 114.51, 109.19, 27.94 (N($\underline{C}H_3$)), 21.34 (–$\underline{C}H_3$); MALDI-TOF: mass calcd for $C_{15}H_{11}BrN_4$ $[M]^+$: 327.18; found $[M]^+$: 327.24, [M+2]: 329.83; Elemental anal. calcd. for $C_{15}H_{11}BrN_4$: C, 55.06; H, 3.39; Br, 24.42; N, 17.12% Found: C, 55.10; H, 3.41; Br, 24.39; N, 17.09%.

*2.2.2g. b 3-chloro-7,10-dimethyl-10H-pyrido[3′,2′:5,6]pyrazino[2,3-b]indole (**7**)* Similar condensation procedure as for **Std** starting from 1,5-dimethylindoline-2,3-dione (200 mg, 1 mmol) and 5-chloropyridine-2,3-diamine (110 mg, 1 mmol). Yellow solid. Yield: 0.199 g (62.11%); M.p.: 244 °C; FT-IR (solid, ν_{max}/cm^{-1}): 3043 (Ar. =C–H str.), 2921; 2856 (Aliph. –C–H str.), 1675 (Ar. –C=N str.), 1603; 1490 (Ar. –C=C str.), 1390 (C–N str.), 1126; 825 (Ar. –C–H bend), 903 (C–Cl); ^{1}H NMR (300 MHz, $CDCl_3$, 25 °C) δ, ppm: 8.79 (d, 1H, H-2, *J* = 1.5 Hz), 8.24 (d, 1H, H-4, *J* = 1.5 Hz), 7.39 (d, 1H, H-6, *J* = 1.5 Hz), 7.26 (d, 1H, ArH, *J* = 7.5 Hz), 7.13 (dd, 1H, ArH, *J* = 1.2 Hz, 1.2 Hz), 3.92 (s, 3H, N($\underline{C}H_3$)), 2.36 (s, 3H, –$\underline{C}H_3$); ^{13}C NMR (75 MHz, $CDCl_3$, 25 °C) δ, ppm: 151.01, 147.35, 147.24, 144.12, 142.60, 141.64, 132.94, 131.73, 130.70, 130.09, 123.41, 123.31, 108.33, 29.66 (N($\underline{C}H_3$)), 21.20 (–$\underline{C}H_3$); MALDI-TOF: mass calcd for $C_{15}H_{11}ClN_4$ $[M]^+$: 282.73; found $[M]^+$: 282.25, [M+2]: 284.73; Elemental anal. calcd. for $C_{15}H_{11}ClN_4$: C, 63.72; H, 3.92; Cl, 12.54; N, 19.82% Found: C, 63.69; H, 3.94; Cl, 12.57; N, 19.79%.

*2.2.2h. b 10-methyl-7-nitro-10H-pyrido[3′,2′:5,6]pyrazino[2,3-b]indole (**8**)* Similar condensation procedure as for **Std** starting from 1-methyl-5-nitroindoline-2,3-dione (200 mg, 1 mmol) and pyridine-2,3-diamine (100 mg, 1 mmol). Red solid. Yield: 0.189 g (70.19%); M.p.: 190 °C; FT-IR (solid, ν_{max}/cm^{-1}): 3058 (Ar. =C–H str.), 2912; 2848 (Aliph. –C–H str.), 1678 (Ar. –C=N str.), 1608; 1485 (Ar. –C=C str.), 1513; 1326 (N–O str.), 1306 (C–N str.), 1071; 843; 739 (Ar. –C–H bend); ^{1}H NMR (300 MHz, $CDCl_3$, 25 °C) δ, ppm: 8.56 (dd, 1H, H-2, *J* = 2.4 Hz, 2.4 Hz), 8.47 (d, 1H, H-6, *J* = 2.4 Hz), 8.12 (dd, 1H, H-8, *J* = 1.5 Hz, 1.5 Hz), 8.01 (dd, 1H, H-4, *J* = 1.5 Hz, 1.5 Hz), 7.58 (d, 1H, H-9, *J* = 7.5 Hz), 7.40 (t, 1H, H-3, *J* = 7.5 Hz, 7.5 Hz), 3.96 (s, 3H, N($\underline{C}H_3$)); ^{13}C NMR (75 MHz, $CDCl_3$, 25 °C) δ, ppm: 158.40, 155.26, 154.62, 149.26, 144.45, 133.69, 130.89, 126.43, 122.96, 121.37, 117.23, 113.74, 110.24, 29.52 (N($\underline{C}H_3$)); MALDI-TOF: mass calcd for $C_{14}H_9N_5O_2$ $[M]^+$: 279.25; found $[M]^+$: 279.19; Elemental anal. calcd. for $C_{14}H_9N_5O_2$: C, 60.21; H, 3.25; N, 25.08; O, 11.46% Found: C, 60.23; H, 3.22; N, 25.10; O, 11.43%.

*2.2.2i. b 3-bromo-10-methyl-7-nitro-10H-pyrido[3′,2′:5,6]pyrazino[2,3-b]indole (**9**)* Similar condensation procedure as for **Std** starting from 1-methyl-5-nitroindoline-2,3-dione (200 mg, 1 mmol) and 5-bromopyridine-2,3-diamine (145 mg, 1 mmol). Orange solid. Yield: 0.295 g (85.13%); M.p.: >250 °C; FT-IR (solid, ν_{max}/cm^{-1}): 3057 (Ar. =C–H str.), 2929; 2852 (Aliph. –C–H str.), 1674 (Ar. –C=N str.), 1608; 1492 (Ar. –C=C str.), 1573; 1336 (N–O str.), 1296 (C–N str.), 1126; 752 (Ar. –C–H bend), 894 (C–Br); ^{1}H NMR (300 MHz, $CDCl_3$, 25 °C) δ, ppm: 8.88 (d, 1H, H-2, *J* = 1.5 Hz), 8.43 (dd, 2H, H-4,6, *J* = 1.5 Hz, 1.5 Hz), 8.12 (dd, 1H, H-8, *J* = 1.5 Hz, 1.5 Hz), 7.58 (d, 1H, H-9, *J* = 7.5 Hz), 3.93 (s, 3H, N($\underline{C}H_3$)); ^{13}C NMR (75 MHz, $CDCl_3$, 25 °C) δ, ppm: 153.01, 150.37, 150.24, 149.17, 144.21, 144.03, 142.25, 133.02, 130.08, 121.68, 121.59, 114.98, 107.64, 29.66 (N($\underline{C}H_3$)); MALDI-TOF: mass calcd for $C_{14}H_8BrN_5O_2$ $[M]^+$: 358.15; found $[M]^+$: 358.64, [M+2]: 360.28; Elemental anal. calcd. for $C_{14}H_8BrN_5O_2$: C, 46.95; H, 2.25; Br, 22.31; N, 19.55; O, 8.93% Found: C, 46.98; H, 2.21; Br, 22.29; N, 19.58; O 8.91%.

*2.2.2j. b 3-chloro-10-methyl-7-nitro-10H-pyrido[3′,2′:5,6]pyrazino[2,3-b]indole (**10**)* Similar condensation procedure as for **Std** starting from 1-methyl-5-nitroindoline-2,3-dione (200 mg, 1 mmol) and 5-chloropyridine-2,3-diamine (110 mg, 1 mmol). Orange solid. Yield: 0.253 g (83.51%); M.p.: 230 °C; FT-IR (solid, ν_{max}/cm^{-1}): 3054 (Ar. =C–H str.), 2920; 2840 (Aliph. –C–H str.), 1673 (Ar. –C=N str.), 1613; 1499 (Ar. –C=C), 1570; 1326 (N–O str.), 1303 (C–N str.), 1099; 752 (Ar. –C–H bend), 985 (C–Cl); ^{1}H NMR (300 MHz, $CDCl_3$, 25 °C) δ, ppm: 8.80 (d, 1H, H-2, *J* = 1.2 Hz), 8.42 (d, 1H, H-6, *J* = 1.5 Hz), 8.25 (d, 1H, H-4, *J* = 1.5 Hz), 8.14 (dd, 1H, H-8, *J* = 1.5 Hz, 1.5 Hz), 7.58 (d, 1H, H-9, *J* = 7.5 Hz); 3.93 (s, 3H, N($C\underline{H_3}$)); ^{13}C NMR (75 MHz, $CDCl_3$, 25 °C) δ, ppm: 151.01, 150.24, 147.35, 147.24, 144.12, 142.25, 141.64, 130.70, 130.09, 121.68, 121.59, 107.64, 29.66 (N($\underline{C}H_3$)); MALDI-TOF: mass calcd for $C_{14}H_8ClN_5O_2$ $[M]^+$: 313.70; found $[M]^+$: 313.55, [M+2]: 315.57; Elemental anal. calcd. for $C_{14}H_8ClN_5O_2$: C, 53.60; H, 2.57; Cl, 11.30; N, 22.33; O, 10.20 % Found: C, 53.63; H, 2.54; Cl, 11.28; N, 22.30; O, 10.24 %.

3. Results and Discussion

3.1 *Synthesis and characterization*

The procedure adopted for the synthesis of **1–10** is presented in Scheme 1. Pyridopyrazino[2,3-*b*]indole derivatives were prepared by simple condensation method using alkylated isatin derivatives and pyridine-2,3-diamine derivatives in glacial acetic acid. Progress of the reaction was monitored by using thin-layer chromatography (TLC) and purity of the compounds were visualized with UV light (365 nm) and in an iodine chamber. The crude product obtained after successful treatment of reaction mixture was employed into column chromatography to separate the regioisomeric product formed using eluent n-hexane:chloroform. After purification, we got the desired product **1–10** in a major quantity and another regioisomer in a minor quantity as reported in the previous study on pyridopyrazino[2,3-*b*]indole molecule.[33,34] The yield of desired major product **1–10** were in the range of 60–86% which was characterized or confirmed through ^{1}H, ^{13}C NMR, IR spectroscopy, Maldi-Tof spectrometry (Figures S6–S28, Supplementary Information) and elemental analysis.

3.2 *Photophysical properties*

In order to examine the relation among photophysical properties of **1–10** with solvent polarity, UV-visible and fluorescence spectra of 10 μM solution prepared in the varying polarity of solvents (toluene, dichloromethane and DMSO) was taken. A further effect of aggregation on UV-visible and fluorescence spectra was investigated by using solid film. Normalized UV-visible absorption spectrum of **1–10** in toluene and the solid film is shown in Figure 1 (for other see Figure S1, Supplementary Information). Pertinent photophysical data are summarized in Table 1 and 2.

The absorption spectra of pyridopyrazino[2,3-*b*]indole (**Std**) display major bands below 400 nm in all solvent, corresponding to n–π* and π–π* transitions. This high energy transition originated from the entire pyridopyrazino[2,3-*b*]indole skeleton. Besides that, charge transfer from electron-donating indole to the electron-accepting pyrido-pyrazine unit originate lower energy transitions above 400 nm, attribute inbuilt intramolecular charge transfer (ICT) which established D–A architecture in pyridopyrazino[2,3-*b*]indole analogs. Similar ground state electronic spectra were observed for substituted pyridopyrazino[2,3-*b*]indole derivatives **1–10** in all solvents (Figure 1 (**a**) and Figure S1, Supplementary Information).

Further, absorption spectra of **1–10** exhibit negligible dependency of ICT transition with increase in solvent polarity ($E_T(30)$) which reveal that the ground-state electronic structures are independent of change in solvent polarity (Figure 1 (**a**), Figure S1 (Supplementary Information) and Table 1).[41,42] However its electronic ground and excited state spectra, found to depend on inductive (+I/−I) or mesomeric (+M/−M) effect exerted by substituted $–CH_3$, –Cl, –Br and $–NO_2$ group and thus show significant red and blue shift (Tables 1 and 2). Often, but not always, mesomeric displacement leads to a shift in ground-state absorption spectra, prevailing over the inductive effect. Though, halogens (–Br/–Cl) having σ electron-withdrawing nature (–I) and π electron-releasing nature (+M effect), but they are the exceptional groups where the inductive effect dominant than the mesomeric effect in its ground state due to poor orbital overlap of halogens with the π-system of an aromatic ring (2p of C and 4p of –Br/3p of –Cl), which prevents any appreciable resonance electron-donation.

Thus, for mono-halo substituted (either at 3rd or at 7th position) compounds (i.e., **1**, **2** and **3**) prevailed, –I capabilities and high electronegativity of –Br/–Cl withdraw electron density away from the ring which leads to a net deactivation of pyridopyrazino[2,3-*b*]indole ring and show hypsochromic shift than **Std** molecule (Figure 1 (**a**) and Table 1).[43–45] As electronic interactions are inverse of electronegativity's of the atoms concerned, being a high electronegative, –Cl

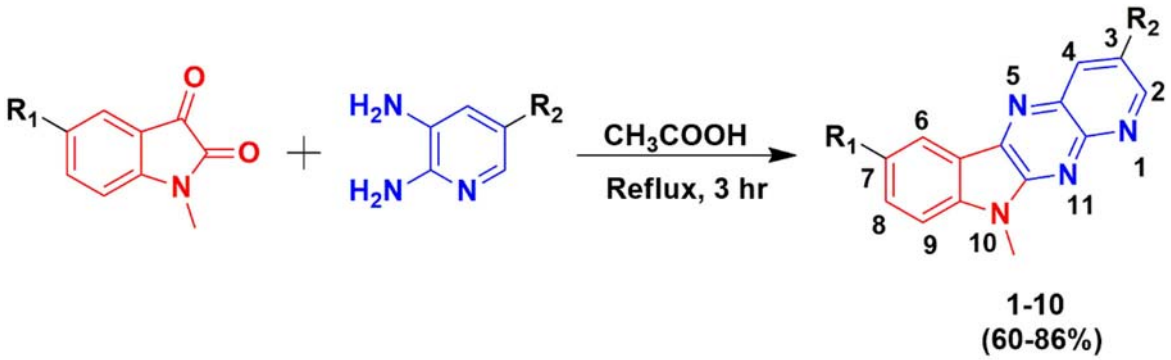

1: R_1 = H, R_2 = Br; **2:** R_1 = Br, R_2 = H; **3:** R_1 = H, R_2 = Cl; **4:** R_1 = Br, R_2 = Cl
5: R_1 = CH_3, R_2 = H; **6:** R_1 = CH_3, R_2 = Br; **7:** R_1 = CH_3, R_2 = Cl
8: R_1 = NO_2, R_2 = H; **9:** R_1 = NO_2, R_2 = Br; **10:** R_1 = NO_2, R_2 = Cl

Scheme 1. Synthetic route of **1–10**.

atom exerts strong –I effect in molecule **3** and thus induces a strong blue shift in ICT than other derivatives.[43,44] Conversely, in case of **4** electron density is not confined in one direction due to presence of two negatively inducting auxochromic group (–Br and –Cl) on opposite arms of pyridopyrazino[2,3-*b*]indole analog, which may result into delocalisation of charges all over the molecule.[43,46] As a result of delocalisation, a slight bathochromic shift of around 2–5 nm was observed in **4** than **Std** (Figure 1 (**a**) and Table 1). However, electron-donating or +I effect possessed by $–CH_3$ group in **5** show 7 nm red shift in ICT than **Std** molecule (Figure 1 (**a**)). Similarly, +I ($–CH_3$) and +M (–Br, –Cl) directing group in **6** and **7** exert slight redshift due to stabilized charge transfer state. Also, strong withdrawing $–NO_2$ substituent (–I/–M directing group) (at 7th position) strongly deactivate the pyridopyrazino[2,3-*b*]indole ring by withdrawing the π-electron density towards itself in **8**, **9** and **10** and thus show blue shifted ICT than **Std**, whereas dual ICT maxima were observed in case of **9** and **10** could be due to the presence of different auxochromic group or the effect of destabilized/highly polarised charge transfer state caused by the presence of opposite effect directing (–I/+M (–Br and –Cl) and –I/–M ($–NO_2$)) group at 3rd and 7th position (Figure 1 (**a**) and Table 1). In addition, observed broader and red-shifted solid-state absorption maxima were a result of intermolecular aggregation (Figure 1 (**b**)).

Photoexcitation of **1–10** at 350 nm originates transition from optically allowed lowest excited state (LE) to charge transfer (CT) state and thereby induces blue–green emission (λ_{max} = 398–527) in solution state (Figure 2 (**a** and **b**), Figure S2 (Supplementary

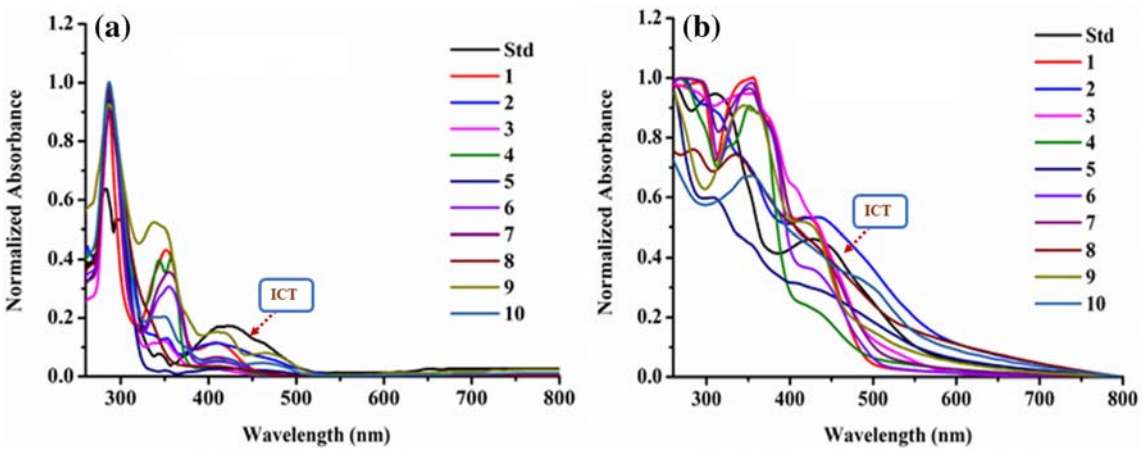

Figure 1. Normalized UV-Vis absorption spectrum of **Std** and **1–10** in (**a**) toluene and (**b**) solid film.

Table 1. Absorption data of 1–10.

Mol.	λ^{a}_{abs}, nm (log $\varepsilon_{max}M^{-1}$ cm^{-1})[b]			λ_{abs}, nm Solid Film
	Toluene	DCM	DMSO	
Std.	298 (3.91), 343 (3.27), 416 (3.39)	260 (4.78), 303 (4.03), 420 (3.61)	262 (4.90), 307 (3.62), 423 (3.50)	312, 429
1	283 (4.59), 352 (4.24), 408 (3.63)	276 (4.62), 350 (4.33), 409 (3.77)	277 (4.42), 353 (4.30), 410 (3.69)	352, 374, 423
2	260 (4.99), 353 (3.44), 412 (3.60)	276 (4.11), 357 (3.44), 416 (3.44)	268 (5.00), 357 (3.44), 417 (3.63)	309, 347, 436
3	286 (5.07), 351 (4.17), 400 (3.61)	275 (4.22), 349 (4.29), 402 (3.83)	286 (3.83), 351 (4.28), 403 (3.83)	354, 427
4	286 (4.74), 342 (4.31), 359 (4.39), 422 (3.20)	274 (4.71), 342 (4.31), 357 (4.32), 422 (3.27)	280 (4.36), 344 (4.75), 361 (4.75), 425 (3.54)	350, 434
5	284 (4.56), 347 (2.95), 423 (2.77)	279 (4.36), 347 (2.95), 428 (2.90)	279 (4.75), 357 (4.48), 430 (3.69)	308, 356, 432
6	286(4.80), 356 (4.29), 421 (3.41)	279 (4.29), 354 (4.35), 423 (3.57)	280 (4.80), 356 (4.29), 424 (3.69)	284, 356, 435
7	285 (4.11), 355(4.45), 418 (3.68)	279 (4.67), 354 (4.49), 421 (4.08)	285 (4.11), 356 (4.75), 423 (3.98)	286, 356, 439
8	285 (4.84), 332 (4.47), 410 (3.17)	279 (4.99), 323 (4.72), 412 (4.03)	287 (4.76), 333 (4.99), 416 (4.24)	288, 337, 448
9	286 (4.23), 338 (3.94), 410 (4.34), 470 (3.00)	270 (4.09), 335 (4.49), 402 (4.02), 473 (2.95)	280 (3.99), 345 (4.99), 405 (3.77), 475 (2.95)	346, 364, 437
10	287 (4.54), 351(3.84), 423 (3.23), 464 (3.11)	264 (4.12), 336 (4.36), 417 (4.58), 465 (4.34)	280 (3.99), 349 (3.98), 412 (4.58), 465 (4.18)	358, 431, 492

[a]Recorded in 10^{-5} M solution, [b]ε is Extinction coefficient (L mol^{-1} cm^{-1}) (in parentheses).

Information) and Table 2). Additional photophysical characteristics, such as the molar extinction coefficient (log ε), optical band gap (E_g^{opt}) (calculated from $\lambda_{opt\text{-}edge}$ obtained from the intersection of excitation and emission spectra), stokes shift (ν_{abs}–ν_{emi}) and fluorescence quantum yield (ϕ_F) (using quinine sulfate (ϕ = 0.54 in 0.5 M H_2SO_4 as a reference) of the molecules were determined (formulae used for calculation of all above entities shown in SI), and the pertinent data are summarized in Tables 1, 2 and Table S1, Supplementary Information. The calculated optical band gap (E_g^{opt}) is in the range of 2.01–2.56 eV (Table 2 and Table S1, Supplementary Information). A significant change in the ground and excited state geometry of molecules and the possibility of formation of charge transfer state in **1–10** were revealed by considerable stokes shift of about 649–3881 cm^{-1} (Table 2 and Table S1, Supplementary Information).

Further, emission property was found to be dependent on increasing solvent polarity from toluene ($E_T(30)$ = 33.9) to DMSO ($E_T(30)$ = 45.0) and show positive solvatochromism with slight bathochromic/red shift in emission maxima (Figure 2 (**a**), (**b**) and Figures S2-S3, Supplementary Information) due to stabilization of enhanced dipole moment of polarized excited state by the polar solvent.[41,42]

As mesomeric effect predominates in electronically excited states than inductive effect due to resonance stabilized dipolar nature of the excited state, so +M property of –Br, –Cl and electron-donating ability of $–CH_3$ in **1–7** lower the potential energy of the excited state and slightly shift their emission maxima towards longer wavelength than **Std** molecule (Figure 2 (**a** and **b**), Figure S2, Supplementary Information (and Table 2)).[43] Besides that, strong electron-withdrawing and –M or –I property of $–NO_2$ substituent in **8** may enhance the potential energy of the excited state via deactivating the ring by withdrawing electron towards itself and exhibit blue-shifted emission maxima.[47,48] Blue-shifted emission in **8** than **Std** may also be associated with the formation of a rigid charged donor-acceptor system due to the presence of electron-withdrawing/deactivating $–NO_2$ substituent.[47] Similar effect was in case of **9** and **10** having $–NO_2$ substituent at 7th position of pyridopyrazino[2,3-*b*]indole but slightly higher and broader emission maxima were observed as compared to **8** due to presence of auxochromic –Br (in **9**) and –Cl (in **10**) substituent at 3rd position (Figure 2 (**a** and **b**), Figure S2, Supplementary Information and Table 2).

However, multiple emission (more than two emission bands) observed for **1–8** in solution state (Figure 2 (**a** and **b**), Figure S2, Supplementary Information) could be the result of (i) an intrinsic emissive property of pyrido-pyrazino[2,3-*b*]indole segment having various conjugated chromophore segment or (ii) vibronic fine structure of the emission band.[45] Nevertheless, some of the derivatives (**1**, **4**, **6**, **7** and **9**) among molecules **1–10** exhibit strong, broader and red-shifted solid film emission maxima (Figure 2 (**c**)) than solution state (Figure 2 (**a** and **b**), Figure S2, Supplementary Information) attribute towards the formation of emissive aggregates. However, other molecules show quenching in solid-state emission (Figure 2 (**c**)), most probably due to fast interchain electron transfer from the donor to acceptor

Table 2. Emission data, optical band gap, stokes shift and quantum yield of **1**–**10**.

Compd.	λ^{a}_{emi}, nm Toluene	DCM	DMSO	λ_{emi}, nm Solid Film	E_g^{opt}eV[b] DCM	Stokes shift, cm^{-1}, (ϕ_f)[c] Toluene
Std	406, 434, 459	406, 433, 463	413, 439, 467	–	2.21	939 (0.40)
1	408, 437, 468	411, 434, 493	414, 440, 524	523	2.12	1395 (0.21)
2	408, 435, 463	408, 434, 463	412, 437, 468	–	2.27	1230 (0.30)
3	411, 435, 461	404, 433, 457	410, 434, 462	–	2.20	1825 (0.49)
4	416, 440, 468	411, 435, 462	418, 440, 471	513	2.21	1558 (0.07)
5	408, 435, 460	407, 430, 461	408, 436, 468	–	2.23	1035 (0.37)
6	411, 435, 462	459	–	528	2.13	939 (0.35)
7	411, 436, 506	428, 455, 527	–	537	2.10	1092 (0.36)
8	398, 423, 449	406, 430, 456	419, 437, 465	–	2.19	762 (0.33)
9	438	476	485	470, 544	2.03	1139 (0.02)
10	444	452	499	–	2.20	1018 (0.38)

[a]Recorded in 10^{-5} M solution, [b]Optical band gap in DCM estimated using emission and excitation spectra $\left(E_g^{opt} = \frac{1240.8}{\lambda_{optedge}}\right)$eV, [c]quantum yield (in parentheses) in toluene with reference to quinine sulphate ($\phi_f = 0.54$ in 0.5 M H_2SO_4).

subunits *via* close spatial contact.[49] The presence of strong solid-state emission in **1**, **4**, **6**, **7** and **9** put forth primary indication of the presence of AIE characteristics than that of counter effect i.e., ACQ in emission and the possible use of these dyes in the fabrication of highly efficient non-doped organic light-emitting diodes (OLED's) or organic nano-dots for bio-imaging application.[1,7]

Consequently, to access AIE characteristic by the formation of aggregates, we chose high solid-state emissive molecules **4**, **7** and **9** (Figure 2 (**c**)). Aggregates of these molecules are formed from simply reported precipitation method[50] using THF/H_2O solvent mixtures and the effect of aggregate formed on the photophysical property was investigated using 10 μM solution of THF/H_2O mixtures with increasing water fraction (vol.%) (f_w) (Figure S4, Supplementary Information). Inbuilt D–A interaction in **4**, **7** and **9** induces strong emission in pure THF solvent on exciting the molecules at their optically allowed LE state to CT state (Figure 3 (**left** and **middle**) and Figure S4, (**right**) Supplementary Information).

While on increase in water (highest polarity ($E_T(30)$ = 63.1)) content in THF-H_2O mixture (upto 60% f_w in **4**, **7** and 50% f_w in **9**) emission intensity reduced (Figure 3 (**left**) and Figure S4 (**right**)) Supplementary Information, due to solvatochromic effect caused by increase in solvent polarity (THF: $E_T(30)$ = 37.4; Water: $E_T(30)$ = 63.1).[21,51] However, it is a well-known fact that organic molecules are highly soluble

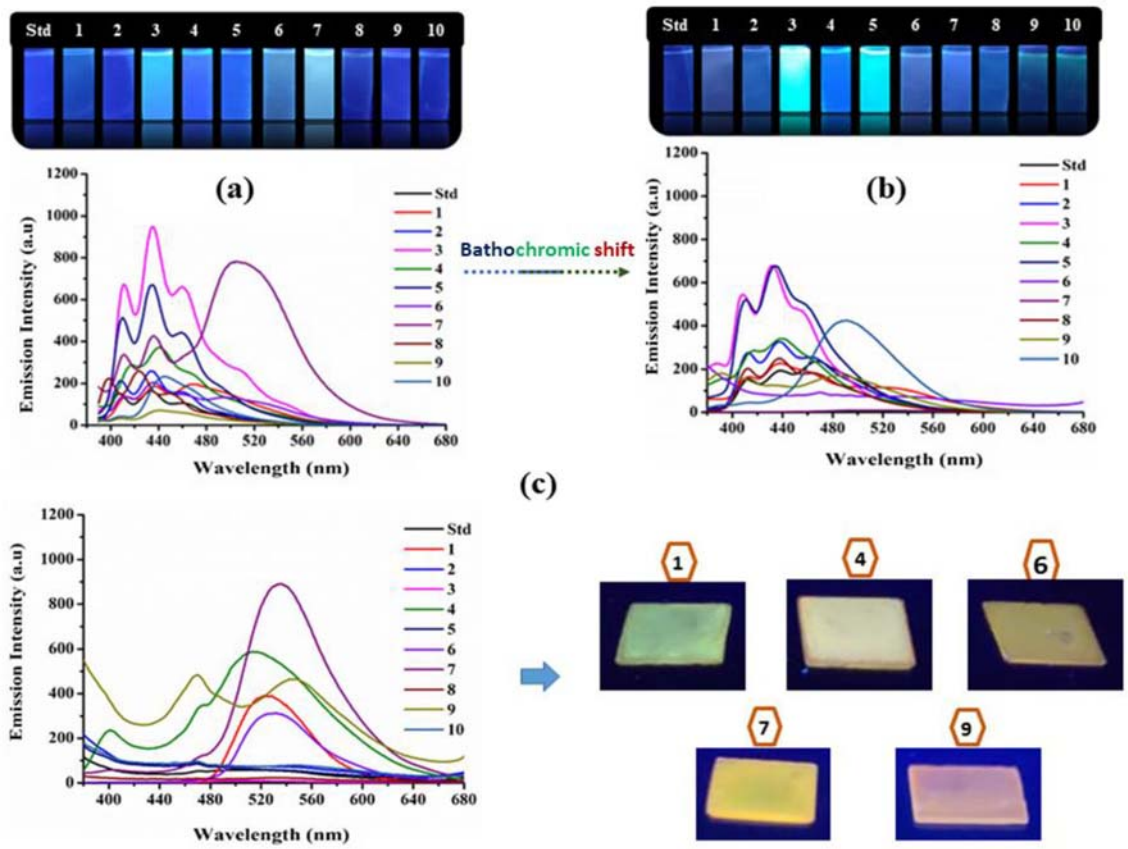

Figure 2. Emission spectra and images of **Std** and **1–10** in (**a**) toluene, (**b**) dichloromethane showing positive solvatochromism and (**c**) solid film emission spectra of **Std** and **1–10** (**left**), solid film images of **1**, **4**, **6**, **7** and **9** (**right**).

in an organic solvent like THF but insoluble in water. As a result, a high percentage of water contents in THF/H_2O solvent mixture creates hydrophobic environment.[21,27,52] Consequently, hydrophobic environment diminishes solvatochromic property and dominates AIE effect in **4**, **7** and **9** by restricting intramolecular rotational (RIR), and vibrational motions as a result, rise in emission intensity (at 70% f_w in **4**, **7** and 60% f_w in **9**) (Figure 3 (**left**) and Figure S4 (**right**), Supplementary Information) was observed with the formation of emissive aggregate particles.[53] However, a further drop of emission intensity in aggregate state at 80%, 90% in **4**, **7** and 70–90% in **9** (Figure 3 (**left**) and Figure S4 (**right**) Supplementary Information) of molecules could be due to the changes in physical constraints of aggregates such as variation in size of particles formed, different conformations, random packing modes and morphological changes of the molecules in the aggregate state and the variable numbers of aggregated particles formed in THF/water mixtures.[10,27,54] In addition, the elimination of solvatochromism by hydrophobic environment tends to experience less polarity by fluorescent aggregate particles in an aggregated state. As a result, their ICT maxima weakened and showed the presence of 'Mie scattering' in UV-Visible spectra of **4**, **7** and **9** (Figure S4 (**left**) (**a–c**), Supplementary Information).[55, 56] Furthermore, low polydispersity indices (PDI) observed in high f_w (70% f_w in **4**, **7** and 60% f_w in **9**) of THF/H_2O mixture from dynamic light scattering (DLS) (Figure 3 (**right**)) study of these molecules confirmed the highly dispersed or homogeneous media with no obvious precipitate in aggregated THF–H_2O mixture and hence implies that the aggregates are of nanoscale, hence called nanoparticles.[27] The hydrodynamic average size of the nanoparticles formed at 70% f_w in THF–H_2O mixture was 184 nm in **4**, 76 nm in **7** and 117 nm in 60% f_w of **9** obtained by DLS (Figure 3 (**right**)). Hence, a rise in emission intensity at the aggregate state of **4**, **7** and **9** implies that molecules are AIE-active and could be used in organic electronic devices as AIE-fluorophores.

3.3 *Electrochemical properties*

Charge-transport capability and feasibility of electron injection or transport in **1–10** were determined by

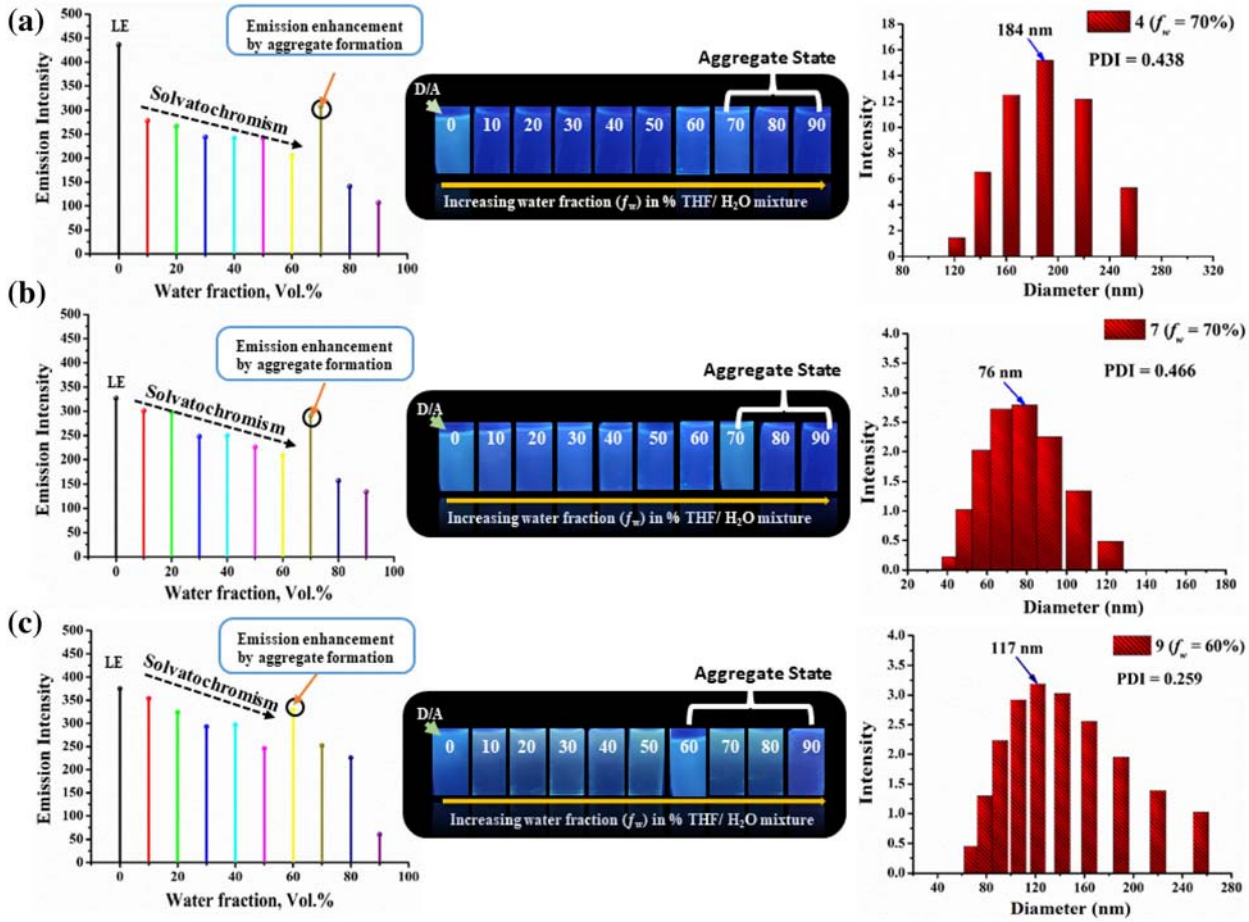

Figure 3. Line plot of emission intensity Vs. an increasing percentage of water in THF–H_2O solvent mixture (**left**), emission images showing AIE effect in THF–H_2O mixture (10 μM) with different % water fraction (f_w) (**middle**) and DLS plot (**right**) of (**a**) **4**, (**b**) **7** and (**c**) **9**.

cyclic voltammetry (CV) in anhydrous dichloromethane solution using ferrocene as an internal standard to calibrate the redox potentials. Cyclic voltammogram of **5** and **9** are shown in Figure 4 (for other see Figure S5, Supplementary Information). The relevant data and HOMO–LUMO energy value are summarised in Table 3 and Figure 5. No significant modification in the repeated scan of the CV measurement reveals the electrochemical stability of molecules under oxidative and reductive conditions.

Oxidation and reduction potential of **1**–**10** display alteration with the presence of –CH_3, –Br, –Cl, –NO_2 group on pyridopyrazino[2,3-*b*]indole (**Std**) which subsequently modify their ionization potential (E_{HOMO}) and electron affinity (E_{LUMO}) (Table 3 and Figure 5). The appearance of two quasi reversible waves around 1.16–1.89 V on anodic sweep indicates oxidation of indole analog in **Std** and **1**–**10** (Table 3). Whereas, one extra lower oxidation potential observed for compounds **3**, **5**, **6**, **7**, **9** and **10** at around 0.85–1.33 V could be due to oxidation of –CH_3, –Cl and –Br (Table 3, Figure 4, Figure S5, Supplementary Information). Further, three quasi reversible waves on cathodic sweep (Table 3) reveal a reduction of pyridopyrazino[2,3-*b*]indole core (**Std**) and similar reduction pattern was observed for all the derivatives **1**–**10** except for **6**, **7** and **8** where two quasi reversible waves observed due to merging of peak. In addition, reducing the propensity of –Cl in **3**, –NO_2 in **9** and **10** display one extra reduction potential (Table 3, Figure 4, Figure S5, Supplementary Information).

The HOMO and LUMO energy levels of molecules indicate interfacial charge transport kinetics of materials in optoelectronic devices. Subsequently calculated HOMO and LUMO energy value from the first oxidation and reduction potentials of **1**–**10** are in the range of −5.08 to −5.75 eV and −3.28 to −3.50 eV, respectively (Figure 5). The electrochemical band gap (1.68–2.47 eV) (Figure 5) are found in accordance with optical band gap (2.03–2.27 eV) (Table 2) of **1**–**10** in DCM solvent. It is clearly evident that the

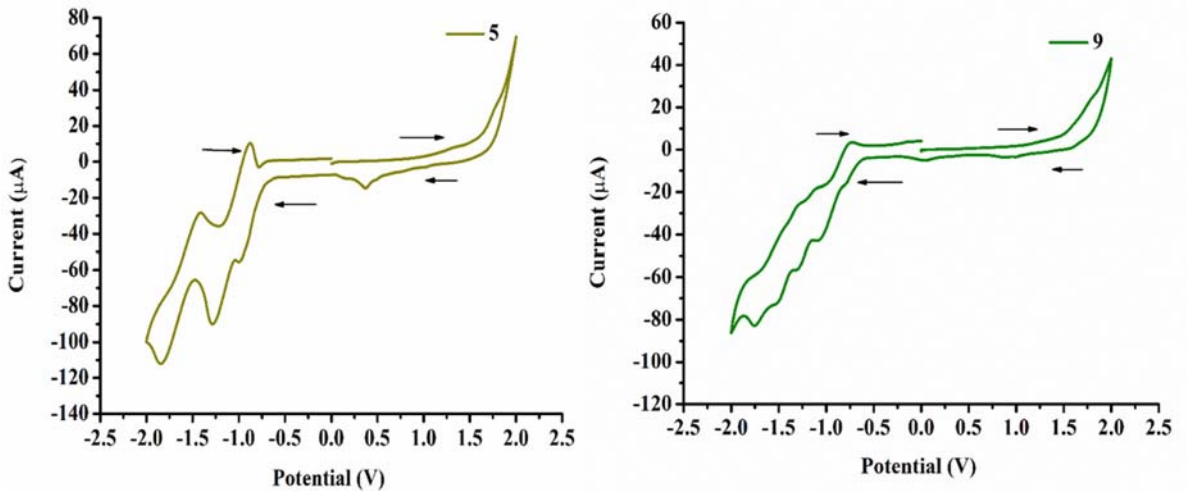

Figure 4. Cyclic voltammogram (full scan) of compound **5** and **9**.

Table 3. Electrochemical and thermal data.

Compd.	E_{oxi}^{peak} [a]	E_{red}^{peak} [b]	T_m (°C)[c]	T_d (°C)[d]
Std	1.59, 1.80	−0.97, −1.28, −1.88	221	167 (183)
1	1.62, 1.83	−1.13, −1.58, −1.77	282	264 (278)
2	1.34, 1.82	−0.95, −1.08, −1.62	198	181 (200)
3	0.85, 1.28, 1.64	−1.04, −1.26, −1.63, −1.80	193	173 (227)
4	1.25, 1.62	−1.05, −1.29, −1.84	241	288 (307)
5	1.33, 1.77, 1.54	−0.97, −1.27, −1.84	172	168 (182)
6	0.95, 1.17, 1.36	−1.04, −1.80	>250	268 (283)
7	1.10, 1.31, 1.80	−1.09, −1.63	244	268 (281)
8	1.16, 1.89	−0.96, −1.78	190	188 (222)
9	1.30, 1.59, 1.80	−1.06, −1.28, −1.50, −1.75	>250	306 (326)
10	0.91, 1.57, 1.83	−1.01, −1.22, −1.39, −1.62	230	294 (318)

[a] E_{oxi}^{peak} oxidation peak potential (V). [b] E_{red}^{peak} reduction peak potential (V). [c] Melting point determined by open capillary method. [d] Decomposition temperature at 5% and 10% (in parentheses) weight loss derived by TGA.

presence of +I or –I group on **Std** (HOMO = −5.80 eV; LUMO = −3.52 eV) moiety effectively shift their corresponding energy levels toward higher potential, thereby increases its hole and electron transporting capability (Figure 5). Consequently, LUMO energy levels of these molecules are found above 3.0 eV and show analogous electron transporting capability than reported n-type organic materials.[1,18,19,25,26,31,57–60]

3.4 *Thermal properties*

In order to check the thermal stability of molecules, **1–10** thermogravimetric analysis (TGA) was carried out at 10 °C min^{-1} under nitrogen atmosphere at normal pressure. Thermograms of **1–10** are displayed in Figure 6 and their pertaining decomposition temperatures are listed in Table 3. Melting points were determined by an open capillary method (Table 3). TGA plot of **1–10** reveals good thermal stability with no weight loss at low temperature.

The thermal decomposition temperatures of **1–10** corresponding to 5% and 10% weight loss are in the ranges of 168 °C to 306 °C and 182 °C to 326 °C, respectively (Table 3). The order of thermal stability of **1–10** is 5 < 3 < 2 < 8 < 1 < 7 < 6 < 4 < 10 < 9 (Table 3). Thus, good thermal stability and high decomposition temperature of molecules could improve the performance of device and exhibit potential usage of it in organic electronics.

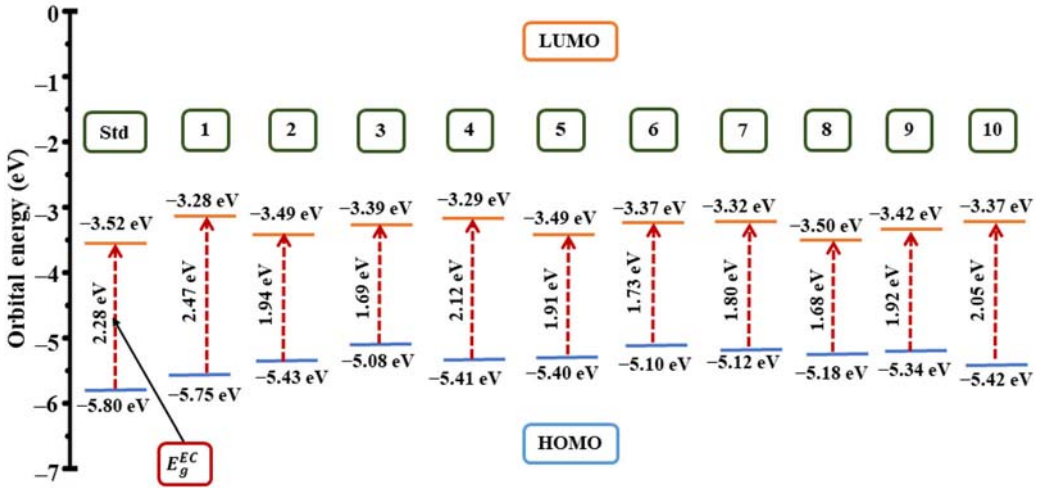

Figure 5. Schematic representation showing correlation between the HOMO and LUMO energies of **Std** and **1–10** as determined from cyclic voltammetry experiment using the equations $E_{HOMO} = -[E_{oxi}^{peak} - E_{redox}\ (Fc/Fc^{+}) + 5.1]$ eV; $E_{LUMO} = -[E_{red}^{peak} - E_{redox}\ (Fc/Fc^{+}) + 5.1]$ eV; E_g^{EC} = [HOMO–LUMO] eV.

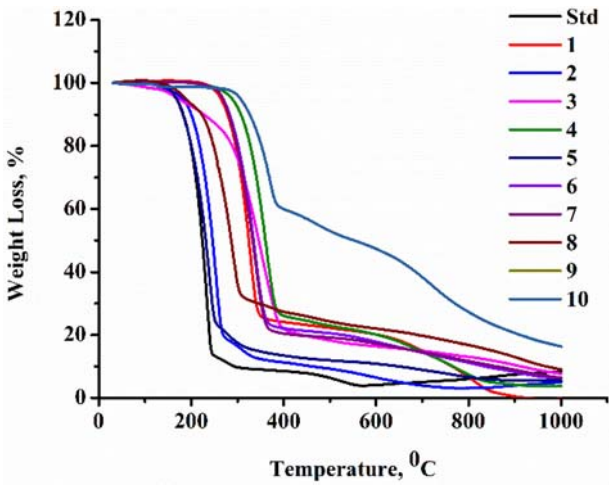

Figure 6. Thermogravimetric plot of **Std** and **1–10**.

4. Conclusions

To conclude, a series of D–A assembly based on pyridopyrazino[2,3-*b*]indole were prepared and their opto-electrochemical properties were effectively studied with modulation of substituent as electron-donating/withdrawing. Inbuilt ICT character possessed by these molecules is responsible for the existence of blue–green emission in the solution state. In addition, some of the molecules display AIE effect due to their strong solid-state emission than solution state which overcomes the ACQ problem and shows the formation of emissive nanoparticles at a high percentage of water in THF/H_2O mixture. Besides that, synthesized compounds show electron-transporting/injecting properties as their electron affinities (LUMO energy levels) are quite comparable to the reported n-type materials. Further, compounds have a high melting point and good thermal stability. Thus, these compounds can be used as solid-state emitter and n-type materials for their application in organic electronics.

Supplementary Information (SI)

SI contains abbreviations, formulae used for calculation of optical characteristics in solution state; UV-vis absorption spectra in DCM and DMSO solvent; emission spectra in DCM and fluorescent images of **Std** and **1–10** in all solvent and in solid film; the method used for AIE experiment, AIE spectra of **4**, **7** and **9**; cyclic voltammogram of **Std** and **1–10**; ^{1}H NMR, ^{13}C NMR, MALDI-TOF and FT-IR spectra of **Std** and **1–10**. Supplementary Information is available at www.ias.ac.in/chemsci.

Acknowledgements

The authors are greatly thankful to Micro-Analytical Laboratory, Department of Chemistry, University of Mumbai, Mumbai for providing instrumental facilities, TIFR-Mumbai for providing MALDI-TOF.

Compliance with ethical standards

Conflict of interest There are no conflicts to declare.

References

1. Tang C W and VanSlyke S A 1987 Organic electroluminescent diodes *Appl. Phys. Lett.* **51** 913
2. Anthony J E 2008 The larger acenes: versatile organic semiconductors *Angew. Chem. Int. Ed.* **47** 452

3. Tao S, Li L, Yu J, Jiang Y, Zhou Y, Lee C S, Lee S T, Zhang X and Kwon O 2009 Bipolar molecule as an excellent hole-transporter for organic-light emitting devices *Chem. Mater*. **21** 1284
4. Kraft A, Grimsdale A C and Holmes A B 1998 Electroluminescent conjugated polymers seeing polymers in a new light *Angew. Chem. Int. Ed.* **37** 402
5. Jenekhe S A and Osaheni J A 1994 Excimers and exciplexes of conjugated polymers *Science* **265** 765
6. Jayanty S and Radhakrishnan T P 2004 Enhanced fluorescence of remote functionalized diaminodicyanoquinodimethanes in the solid state and fluorescence switching in a doped polymer by solvent vapors *Chem. Eur. J*. **10** 791
7. Jares-Erijman E A and Jovin T M 2003 FRET imaging *Nat. Biotechnol.* **21** 1387
8. Luo J, Xie Z, Lam J W Y, Cheng L, Chen H, Qiu C, Kwok H S, Zhan X, Liu Y, Zhu D and Tang B Z 2001 Aggregation-induced emission of 1-methyl-1,2,3,4,5-pentaphenylsilole *Chem. Commun.* **18** 1740
9. Hong Y, Lama J W Y and Tang B Z 2009 Aggregation-induced emission: phenomenon, mechanism and applications *Chem. Commun.* **29** 4332
10. Hong Y, Lam J W Y and Tang B Z 2011 Aggregation-induced emission *Chem. Soc. Rev.* **40** 5361
11. Sakamoto Y, Suzuki T, Kobayashi M, Gao Y, Fukai Y, Inoue Y, Sato F and Tokito S 2004 Perfluoropentacene: High-Performance p–n junctions and complementary circuits with pentacene *J. Am. Chem. Soc.* **126** 8138
12. Liang Z, Tang Q, Xu J and Miao Q 2011 Soluble and Stable N-Heteropentacenes with High Field-Effect Mobility *Adv. Mater.* **23** 1535
13. Thomas K R J, Lin J T, Tao Y T and Ko C W 2001 Light-emitting carbazole derivatives: potential electroluminescent materials *J. Am. Chem. Soc.* **123** 9404
14. Zhuang J, Su W, Li W, Zhou Y, Shen Q and Zhou M 2012 Configuration effect of novel bipolar triazole/carbazole-based host materials on the performance of phosphorescent OLED devices *Org. Electron.* **13** 2210
15. Thomas K R J, Lin J T, Tao Y T and Chuen C H 2002 Quinoxalines incorporating triarylamines: potential electroluminescent materials with tunable emission characteristics *Chem. Mater.* **14** 2796
16. Chang D W, Ko S J, Kim J Y, Dai L and Baek J B 2012 Multifunctional quinoxaline containing small molecules with multiple electron-donating moieties: Solvatochromic and optoelectronic properties *Synth. Met.* **162** 1169
17. Shaikh A M, Sharma B K and Kamble R M 2015 Synthesis, Photophysical, Electrochemical and Thermal Studies of Triarylamines based on benzo[*g*]quinoxalines *J. Chem. Sci.* **127** 1571
18. Shaikh A M, Sharma B K and Kamble R M 2016 Electron-deficient molecules: photophysical, electrochemical, and thermal investigations of naphtho[2,3-*f*]quinoxaline-7,12-dione derivatives *Chem. Heterocycl. Compd.* **52** 110
19. Shaikh A M, Sharma B K, Chacko S and Kamble R M 2016 Synthesis and optoelectronic investigations of triarylamines based on naphtho[2,3-*f*]quinoxaline-7,12-dione core as donor–acceptors for n-type materials *RSC Adv.* **6** 60084
20. Kanekar D N, Chacko S and Kamble R M 2019 Quinoxaline based amines as blue-orange emitters: Effect of modulating donor system on optoelectrochemical and theoretical properties *Dyes Pigm.* **167** 36
21. Singh P S, Chacko S and Kamble R M 2019 The design and synthesis of 2,3-diphenylquinoxaline amine derivatives as yellow-blue emissive materials for optoelectrochemical study *New J. Chem.* **43** 6973
22. Mahadik S S, Chacko S and Kamble R M 2019 2,3-Di(thiophen-2-yl)quinoxaline Amine Derivatives: Yellow-Blue Fluorescent Materials for Applications in Organic Electronics *ChemistrySelect* **4** 10021
23. Przyjazna B, Kucybała Z and Czkowski J P 2004 Development of new dyeing photoinitiators based on 6*H*-indolo[2,3-*b*]quinoxaline skeleton *Polymer* **45** 2559
24. Thomas K R J and Tyagi P 2010 Synthesis, Spectra, and Theoretical Investigations of the Triarylamines Based on 6H-indolo[2,3-*b*]quinoxaline *J. Org. Chem.* **75** 8100
25. Sharma B K, Shaikh A M, Chacko S and Kamble R M 2017 Synthesis, Spectral, Electrochemical and Theoretical Investigation of indolo[2,3-*b*]quinoxaline dyes derived from Anthraquinone for n–type materials *J. Chem. Sci.* **129** 483
26. Kamble R M, Sharma B K, Shaikh A M and Chacko S 2018 Design, Synthesis, Opto–Electrochemical and Theoretical Investigation of Novel Indolo[2, 3-*b*]naphtho[2, 3-*f*]quinoxaline Derivatives for n–Type Materials in Organic Electronics *ChemistrySelect* **3** 6907
27. Singh P S, Badani P M and Kamble R M 2019 Impact of the donor substituent on the optoelectrochemical properties of 6*H*-indolo[2,3-*b*]quinoxaline amine derivatives *New J. Chem.* **43** 19379
28. Kim R, Oh D H, Hwang M C, Baek J Y, Shin S C, Kwon S K and Kim Y H 2012 New Pyridopyrazine Skelecton-Based Electron-Transporting Materials *J. Nanosci. Nanotechnol.* **12** 4370
29. Zhao H, Wei Y, Zhao J and Wang M 2014 Three donor-acceptor polymeric electrochromic materials employing 2,3-bis(4-(decyloxy)phenyl)pyrido[4,3-*b*]pyrazine as acceptor unit and thiophene derivatives as donor units *Electrochim. Acta* **146** 231
30. Okamoto T, Terada E, Kozaki M, Uchida M, Kikukawa S and Okada K 2003 Facile synthesis of 5,10-diaryl-5,10-dihydrophenazines and application to EL devices *Org. Lett.* **5** 373
31. Kanekar D N, Chacko S and Kamble R M 2018 Synthesis, Opto-electrochemical and Theoretical Investigation of Pyrazino[2,3-*b*]phenazine Amines for Organic Electronics *ChemistrySelect* **3** 4114
32. Kanekar D N, Chacko S and Kamble R M 2020 Synthesis and investigation of the photophysical, electrochemical and theoretical properties of phenazine–amine based cyan blue-red fluorescent materials for organic electronics *New J. Chem.* **44** 3278
33. Buu-Hoi N P and Saint-Ruf G 1960 Condensation of isatins with asymmetric aromatic and heterocyclic o-diamines *Bull. Soc. Chim. Fr.* 1920
34. Bergman J and Charlotta D 1996 Synthesis of pyridopyrazino[2,3-*b*] indoles and 10*H*-indolo [3,2-*g*]pteridins *Recl. Trav. Chim. Pays-Basb.* **115** 31
35. Andrieu B M and Mdrour J Y 1998 Reactions of 3-([(Trifluoromethyl)sulfonyl]oxy)-l*H*-indole derivatives

with diamines and carbon nucleophiles. Synthesis of 6*H*-Indolo[2,3-*b*]quinoxaline derivatives *Tetrahedron* **54** 11095
36. Alphonse F A, Routier S, Coudert G and Merour J Y 2001 A straightforward synthesis of pyridopyrazino[2,3-*b*]indoles and indolo[2,3-*b*]Quinoxaline *Heterocycles* **55** 925
37. Jamrozy K, Szymoniak K and Ostrowska K 2008 The regioselective synthesis of 2*H*-pyrido[2,3-*b*]pyrrolo[2,3-*e*]pyrazin-2-one *Heterocycles* **75** 2275
38. Dandia A, Parewa V, Maheshwari S and Rathore K S 2014 Cu doped CdS nanoparticles: A versatile and recoverable catalyst for chemoselective synthesis of indolo[2,3-*b*]quinoxaline derivatives under microwave irradiation *J. Mol. Catal. A Chem.* **394** 244
39. Seth M, Bhaduri A P, Khanna N M and Dhar M L 1974 Antiamoebic agents. Syntheses of substituted indophenazines, azaindophenazines, and azaquinoxalines *Indian J. Chem.* **12** 124
40. Beauchard A, Ferandin Y, Frere S, Lozach O, Blairvacq M, Meijer L, Thiery V and Besson T 2006 Synthesis of novel 5-substituted indirubins as protein kinases inhibitors *Bioorg. Med. Chem.* **14** 6434
41. Reichardt C 1979 Empirical parameters of solvent polarity as linear free-energy relationships *Angew. Chem. Lnt. Ed. Engl.* **18** 98
42. Reichardt C 1994 Solvatochromic dyes as solvent polarity indicators *Chem. Rev.* **94** 2319
43. Forbes W F and Audrey S R 1956 Light Absorption Studies: Part V. The Relation Of Mesomeric Effects And Ultraviolet Light Absorption Spectra *Can. J. Chem.* **34** 1447
44. Lohmann W 1974 Halogen-substitution effect on the optical absorption bands of uracil *Z. Naturforsch.* **29** 493
45. Law K Y 1987 Squaraine chemistry: effects of structural changes on the absorption and multiple fluorescence emission of bis[4-(dimethylamino)phenyl]squaraine and its derivatives *J. Phys. Chem.* **91** 5184
46. D'Aleo A, Saul A, Attaccalite C and Fages F 2019 Influence of halogen substitution on aggregation-induced near infrared emission of borondifluoride complexes of 2′-hydroxychalcones *Mater. Chem. Front.* **3** 86
47. Norman S A, Michele E, Femando C, Teresa C, Maria B P and Arthur G 1997 Photochemistry and photocuring activities of novel substituted 4′-(4-methylphenylthio) benzophenones as photoinitiators *J. Photochem. Photobiol. A* **110** 183
48. Pant G J N, Singha P, Rawat B S, Rawat M S M and Joshi G C 2011 Synthesis, characterization and fluorescence studies of 3,5-diaryl substituted 2-pyrazolines *Spectrochim. Acta A* **78** 1075
49. Sun S S and Carl E B 2005 In *Organic Photovoltaics: Mechanisms, Materials, and Device* S S Sun and N S Sariciftci (Eds.) (Boca Raton: CRC Press/Taylor and Francis) p.183
50. Kasai H, Nalwa H S, Oikawa H, Okada S, Matsuda H, Minami N, Kakuta A, Ono K, Mukoh A and Nakanishi H 1992 A Novel Preparation Method of Organic Microcrystals *Jpn. J. Appl. Phys.* **31** L1132
51. Yang Z W, Qin W Y L, Jacky S, Chen H Y, Herman D W I and Tang B Z 2013 Fluorescent pH sensor constructed from a heteroatom-containing luminogen with tunable AIE and ICT characteristics *Chem. Sci.* **4** 3725
52. Luis S A, Manuela M, Bjorn O R and Roland L 1995 Theoretical Study of the Internal Charge Transfer in Aminobenzonitriles *J. Am. Chem. Soc.* **117** 3189
53. Mei J, Leung N L C, Kwok R T K, Lam J W Y and Tang B Z 2015 Aggregation-induced emission: together we shine, united we soar! *Chem. Rev.* **115** 11718
54. Luo X, Li J, Li C, Heng L, Dong Y Q, Liu Z, Bo Z and Tang B Z 2011 Reversible switching of the emission of diphenyldibenzofulvenes by thermal and mechanical stimuli *Adv. Mater.* **23** 3261
55. Tang B Z, Geng Y, Lam J W Y, Li B, Jing X, Wang X, Wang F, Pakhomov A and Zhang X X 1999 Processible Nanostructured Materials with Electrical Conductivity and Magnetic Susceptibility: Preparation and Properties of Maghemite/Polyaniline Nanocomposite Films *Chem. Mater.* **11** 1581
56. Mei J, Wang J, Sun J Z, Zhao H, Yuan W, Deng C, Chen S, Herman H Y S, Lu P, Qin A, Kwok H S, Ma Y, Williams I D and Tang B Z 2012 Siloles symmetrically substituted on their 2,5-positions with electron-accepting and donating moieties: facile synthesis, aggregation-enhanced emission, solvatochromism, and device application *Chem. Sci.* **3** 549
57. Fukuda T, Kanbara T, Yamamoto T, Ishikawa K, Takezoe H and Fukuda A 1996 Polyquinoxaline as an excellent electron injecting material for electroluminescent device *Appl. Phys. Lett.* **68** 2346
58. Tonzola C J, Alam M M, Kaminsky W and Jenekhe S A 2003 New n-Type Organic Semiconductors: Synthesis, Single Crystal Structures, Cyclic Voltammetry, Photophysics, Electron Transport, and Electroluminescence of a Series of Diphenylanthrazolines *J. Am. Chem. Soc.* **125** 13548
59. Usta H, Facchetti A and Marks T J 2011 n-Channel Semiconductor Materials Design for Organic Complementary Circuits *Acc. Chem. Res.* **44** 501
60. Sharma B K, Shaikh A M, Chacko S and Kamble R M 2018 Synthesis and optoelectronic investigation of triarylamines based on imidazoanthraquinone as donor–acceptors for n-type materials *J. Chem. Sci.* **130** 49